Received: 6 August 2024 | Revised: 10 October 2024 | Accepted: 15 October 2024

DOI: 10.1002/cyto.a.24904

ORIGINAL ARTICLE

MIFlowCyt

ISAC INTERNATIONAL SOCIETY FOR ADVANCEMENT OF CYTOMETRY

CYTOMETRY Journal of Quantitative Cell Science PART A

Overcoming fixation and permeabilization challenges in flow cytometry by optical barcoding and multi-pass acquisition

Marissa D. Fahlberg[1] | Sarah Forward[1] | Emane Rose Assita[1] | Michael Mazzola[2,3,4] | Anna Kiem[2,3,4] | Maris Handley[2] | Seok-Hyun Yun[5] | Sheldon J. J. Kwok[1]

[1]LASE Innovation Inc., Waltham, Massachusetts, USA

[2]Center for Regenerative Medicine, Massachusetts General Hospital, Boston, Massachusetts, USA

[3]Harvard Stem Cell Institute, Cambridge, Massachusetts, USA

[4]Department of Stem Cell and Regenerative Biology, Harvard University, Cambridge, Massachusetts, USA

[5]Wellman Center for Photomedicine, Massachusetts General Hospital, Boston, Massachusetts, USA

Correspondence
Sheldon J.J. Kwok, LASE Innovation Inc., Waltham, Massachusetts, USA.
Email: skwok@laseinno.com

Funding information
National Institutes of Health, Grant/Award Numbers: R44-GM139504, R43-GM140527, R01-EB033155, F31HL158020-03, T32GM132089-01, 5T32GM007226-43

Abstract

The fixation and permeabilization of cells are essential for labeling intracellular biomarkers in flow cytometry. However, these chemical treatments often alter fragile targets, such as cell surface and fluorescent proteins (FPs), and can destroy chemically-sensitive fluorescent labels. This reduces measurement accuracy and introduces compromises into sample workflows, leading to losses in data quality. Here, we demonstrate a novel multi-pass flow cytometry approach to address this long-standing problem. Our technique utilizes individual cell barcoding with laser particles, enabling sequential analysis of the same cells with single-cell resolution maintained. Chemically-fragile protein markers and their fluorochrome conjugates are measured prior to destructive sample processing and adjoined to subsequent measurements of intracellular markers after fixation and permeabilization. We demonstrate the effectiveness of our technique in accurately measuring intracellular FPs and methanol-sensitive antigens and fluorophores, along with various surface and intracellular markers. This approach significantly enhances assay flexibility, enabling accurate and comprehensive cellular analysis without the constraints of conventional one-time measurement flow cytometry. This innovation paves new avenues in flow cytometry for a wide range of applications in immuno-oncology, stem cell research, and cell biology.

KEYWORDS
fixation and permeabilization, flow cytometry, fluorescent protein, intracellular assays, laser particles, optical barcoding, phospho-flow, single cell

1 | INTRODUCTION

Over the past few decades, the scope of cell markers measured by flow cytometry has expanded from surface antigens to various intracellular proteins, such as cytokines and fluorescent reporter proteins, and intranuclear and genetic targets [1–10]. This expansion has enhanced the utility of flow cytometry across immunology and immuno-oncology [11–14], stem cell research [15–17], and cell biology [18–20]. For comprehensive phenotypic and functional analysis in these fields, it is essential to measure both surface and intracellular markers. However, cell processing for these measurements is challenging and can introduce significant measurement errors. For instance, fluorescent proteins (FPs) are commonly used to track gene uptake and expression, but fixation and permeabilization required to detect intracellular markers can cause physical loss and chemical alteration of intracellular FPs. Anti-green fluorescent protein (GFP) antibodies can be used to mitigate this issue [21–23], but they are often inadequate to recover the full signal from FPs. Similarly, when detecting phosphorylated proteins, methanol permeabilization damages the antigen epitopes of surface markers [24–27], which are crucial for

understanding cell signaling and immune response. These marker-destructive sample processing steps complicate assay design and prevent optimal detection of markers.

Recently, we introduced multi-pass flow cytometry, which enables multiple measurements of the same cells using laser particles (LPs) as optical cell barcodes [28]. LPs are semiconductor-based optical probes that emit narrowband (<0.2 nm) laser emission anywhere between 1100 and 1600 nm when pumped by a 1064 nm laser. Given 1000 possible distinguishable wavelengths of LPs, a cell with 3 or more LPs is considered barcoded since there are $>10^8$ potential combinations of spectral patterns. LPs are attached to cells either through non-specific uptake or through an antibody toward a pan-expressing marker (e.g. beta-2-microglobulin). With integration of an infrared spectrometer, LP-barcoded cells can be read on a flow cytometer with no interference with conventional fluorescent probes. In our previous study, we demonstrated a multi-pass workflow in which cells are measured sequentially. With each measurement, different sets of markers are measured, and the data acquired are combined for each cell based on its unique barcode. We used this workflow to acquire a 32-marker panel targeting surface markers with live PBMCs, as well as time-resolved single-cell measurements of T-cell activation [28].

Here, we show that multi-pass flow cytometry also offers effective solutions to long-standing difficulties associated with fixation, permeabilization, and methanol treatments in conventional flow cytometry. The key innovation enabled by cell barcoding is the ability to acquire sensitive and fragile markers first under optimal conditions. The sample is then processed for intracellular markers using methods which may be destructive to those measured in the first pass. The acquired data from the same cells through sequential flow cytometry are combined using the LP cell barcodes [28, 29]. We demonstrate the compelling need for this approach and its effectiveness in three applications that require accurate measurement of methanol-sensitive epitopes, protein-based fluorophores, and FPs in conjunction with harsh cell processing. Our method enables the detection of a wide range of previously incompatible marker types without compromise and risk of quantification errors.

2 | MATERIALS AND METHODS

2.1 | Isolation of bone marrow cells from mice

All mice used in this study were maintained at Massachusetts General Hospital in a temperature- and humidity-controlled environment with a 12-h light / 12-h dark cycle and provided with food and water *ad libitum*. C57Bl/6-CAG-mRFP1-IRES-GFP mice, aged 8–12 weeks, were generated as previously described at the Harvard Genome Modification Facility [30]. The knock-in construct was modified from pR26CAG/GFP Dest (#74286, Addgene) by VectorBuilder to include a bicistronic fluorescent reporter encoding both mRFP and eGFP. Bone marrow cells were collected by crushing the tibias, femurs, hips, humeri, and spine of the mice. After collection, lineage cells were depleted with a lineage cell depletion kit (#130–090-858, Miltenyi Biotec) according to the manufacturer's instructions. Enriched progenitors and hematopoietic stem cells were then utilized for further analysis. All experiments involving mice were conducted under the approval of the Institutional Animal Care and Use Committee at Massachusetts General Hospital (IACUC protocol #2016 N000085).

2.2 | MCF7 cell culture and intranuclear staining

MCF7 GFP- and GFP+ cell lines were sourced from ATCC (Manassas, VA) and GenTarget (San Diego, CA), respectively. These cells were cultured in MCF7 media (Minimal Essential Medium with 10% fetal bovine serum [FBS], 1% Penicillin/Streptomycin [P/S], 1% sodium pyruvate, and 1% non-essential amino acids [all (v/v)]) in T75 flasks. Culturing was timed to allow passaging 1 day before experiment harvest. For detachment, 0.25% Trypsin ethylenediaminetetra-acetic acid (EDTA) was used and neutralized with MCF7 media. Cells were seeded into 12-well plates at $\sim 1.5 \times 10^5$ cells/cm^2, adjusting the volume to 2 mL per well with MCF7 media. Plates were incubated overnight at 37°C with 5% CO_2. After incubation, cells were harvested, counted, and allocated at $\sim 5 \times 10^5$ cells per tube for each sample, reserving some GFP- and GFP+ cells as compensation controls.

For intranuclear staining, MCF7 cells were treated with a Foxp3/Transcription Factor Staining Buffer Set (eBioscience™) following the manufacturer's recommendations. In brief, samples were fixed and permeabilized with Foxp3 Fixation/Permeabilization working solution for 45 min at 4°C and washed twice with 1X Permeabilization Buffer prior to intracellular staining.

2.3 | Multi-pass phospho-flow protocol

Cryopreserved human peripheral blood mononuclear cells (hPBMCs) were thawed and incubated in 0.1 mg/mL bovine pancreatic DNase I (STEMCELL) in Roswell Park Memorial Institute (RPMI) 1640 medium for 15 min at room temperature to mitigate cell clumping. Next, the hPBMCs were washed and resuspended in a 1:1000 dilution of LIVE/DEAD™ Fixable Green Dead Cell Stain Kit (Invitrogen™) in phosphate buffered saline (PBS), and incubated for 30 min in the dark at room temperature. The hPBMCs were then washed and resuspended in 325 µL of PBMC media (20% FBS (v/v), 1% P/S (v/v) in RPMI 1640). The cells were stimulated with 1X Cell Stimulation Cocktail (eBioscience™), composed of PMA/Ionomycin, at 37°C for 15 min. After stimulation, the cells were immediately fixed by the addition of 200 µL of 4.2% formaldehyde (w/w) for 30 min at room temperature. Cells were washed in 2 mL of PBS, followed by another wash in 2 mL of wash buffer (10% FBS (v/v), 10 mM 2-[4-(2-hydroxyethyl)piperazin-1-yl]ethanesulfonic acid (HEPES) buffer, 2 mM EDTA, 1X poloxamer 188 non-ionic surfactant (Gibco™) in PBS) at 600 g for 5 min each. Cells were then aliquoted into sample tubes for barcoding with LPs.

hPBMCs used in the phospho-flow protocol were barcoded after stimulation and fixation, prior to surface staining with antibodies. For

barcoding, hPBMCs were stained with biotinylated antibodies against CD45 and β2-microglobulin (BioLegend) during a 15-min incubation at 4°C. After washing, cells were resuspended in 1 mL of wash buffer. Streptavidin-coated LPs were added at a 10:1 LP:cell ratio. Samples were mixed using a HulaMixer™ (Invitrogen™) at 4°C for 30 min, centrifuged at 600 g for 5 min, and the supernatant was discarded.

In 100 µL of wash buffer, samples were stained with an antibody panel targeting major cell populations (see Table S1) in the dark at room temperature for 20 min. Following washing, samples were acquired and captured using a LASE multi-pass flow cytometer at a medium flow rate (30 µL/min). Captured samples were then fixed with 900 µL ice-cold methanol while vortexing, incubated on ice for 30 min, washed with PBS and wash buffer, and stained with p-ERK1/2 for 25 min in the dark at room temperature. After a final wash, cells were resuspended in 100 µL of wash buffer, and data from the second pass were acquired at a slower flow rate (10 µL/min) to maximize signal-to-noise.

2.4 | Multi-pass GFP / cell cycle protocol with MCF7 GFP+ and bone marrow cells

MCF7 cells were barcoded prior to staining with a 1:1000 dilution of LIVE/DEAD™ Fixable Near-IR Dead Cell Stain Kit (Invitrogen™) in PBS for 30 min in the dark. To barcode, cells were harvested and resuspended in 100 µL of 0.1 mg/mL bovine pancreatic DNase I in RPMI 1640. A batch of polyethyleneimine (PEI) polymer-coated LPs were added to samples in 5 mL Eppendorf tubes once every 15 min, totaling to 4 additions, to achieve a final 10:1 LP:cell ratio. During this time, the sample tubes were mixing on an Eppendorf ThermoMixer® C at 300 rpm for 60 min at room temperature to facilitate the uniform, stochastic adhesion of LPs on the cell surface.

Mouse bone marrow cells were barcoded after antibody staining for lineage antibodies CD8A, CD3E, CD45R, GR1, CD11b, Ter119, and CD4 all conjugated to Alexa Fluor 700 (Table S1). To barcode, samples were resuspended in 100 µL of wash buffer containing a cocktail of biotinylated antibodies targeting progenitors and hematopoietic stem cells [H-2 kb/H-2Db (Invitrogen™), CD105 (eBioscience™), CD150, CD45, and CD41 (BioLegend)] and incubated for 15 min at 4°C. After washing, samples were incubated in 100 µL of wash buffer containing 10 µg of purified streptavidin (BioLegend) for 25 min at 4°C. After a final wash, samples were resuspended in 1 mL of wash buffer. Biotin-coated LPs were added at a 10:1 LP:cell ratio. Samples were mixed at 5-min intervals, alternating between centrifugation and thermo-mixing at 4°C for a total of 30 min. Finally, the cells were stained with viability dye.

All cells were acquired on a LASE multi-pass flow cytometer at a flow rate of 30 µL/min for the first pass, followed by cell capture. Captured samples were fixed and permeabilized in 250 µL of BD Fixation/Permeabilization solution (4.2% formaldehyde (w/w)) on ice for 20 min. The samples were washed and resuspended in 750 µL of 1X BD Perm/Wash™ Buffer and centrifuged at 400 g for 5 min. Each pellet was resuspended in 500 µL of 1X BD Perm/Wash™ Buffer, then stained with either Ki67-Alexa Fluor® 555 or Ki67-PE for 30 min in the dark on ice. Samples were washed with 500 µL of 1X BD Perm/Wash™ Buffer and centrifuged at 400 g for 5 min. The pellets were resuspended in 500 µL of a 1:2500 dilution of 4′,6-diamidino-2-phenylindole (DAPI) in 1X BD Perm/Wash™ Buffer and incubated in the dark on ice for 10 min. The samples were centrifuged at 400 g for 5 min and resuspended in 100 µL of wash buffer prior to a second acquisition at a flow rate of 10 µL/min.

2.5 | Data analysis

Barcoded data were aligned using a proprietary matching algorithm and then exported as Flow Cytometry Standard (FCS) files for analysis using FlowJo version 10.10.0. Single-color compensation controls for all fluorescent antibodies, viability stains, DAPI, and fluorescent reporters were used for all experiments. Cytometer detector gains were set using detector setting incrementation to optimize the signal levels from single-color controls. Compensation controls were either as bright as or brighter than the corresponding samples. Compensation matrices from each pass were generated individually, automatically calculated with minimal manual modifications, and subsequently joined and applied to barcoded data for analysis. Specifically, to join an $[m \times m]$ compensation matrix from a first pass with an $[n \times n]$ matrix from a second pass, an $[(m + n) \times (m + n)]$ matrix was generated with compensation values set to zero for off-diagonal elements as there is no spectral overlap between fluorescence signals acquired in different passes [28].

Data transformation and plotting were implemented using R software and the 'tidyverse' and 'ggcyto' packages [31–33]. A minimum of 100,000 events were collected per acquisition, with live single cells gated for subsequent analyses. In barcoded samples, only cells with a high statistical confidence of matching (<5% error) were selected. For phospho-flow cytometry studies, gating was based on isotype controls and non-stimulated sample data. In experiments involving GFP and mRFP1, gating strategies were established using GFP-negative MCF7 cells and wild-type (non-reporter) mice as references. The calculation of FP loss was conducted directly within FlowJo using the ratio of GFP and mRFP1 signals between the first and second passes.

3 | RESULTS

3.1 | LP cell barcoding is compatible with harsh sample processing

We evaluated the effectiveness of multi-pass flow cytometry for measuring sets of distinctive markers that require competing sample processing and cell staining methods. Specifically, we investigated protocols requiring fixation and permeabilization, which are essential for staining DNA content, intranuclear proteins like transcription factors, phosphorylated proteins, and detecting FPs within the cytoplasm. Figure 1A shows a general workflow schematic. Cells are

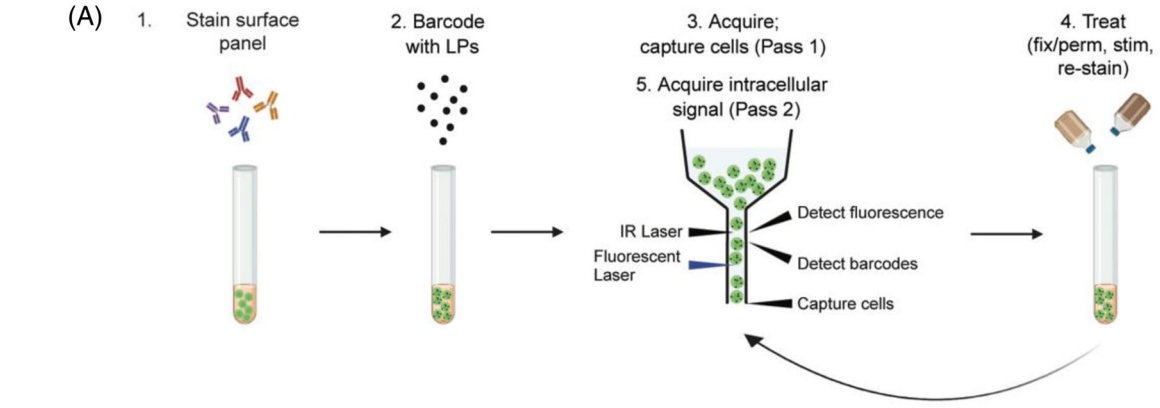

(B)

Application	Fix/perm
Cell Cycle	4.2% FA/saponin
Intranuclear	eBio FoxP3 kit 1-5% FA/0.1-1% MeOH
P-flow	1.6% FA/100% MeOH

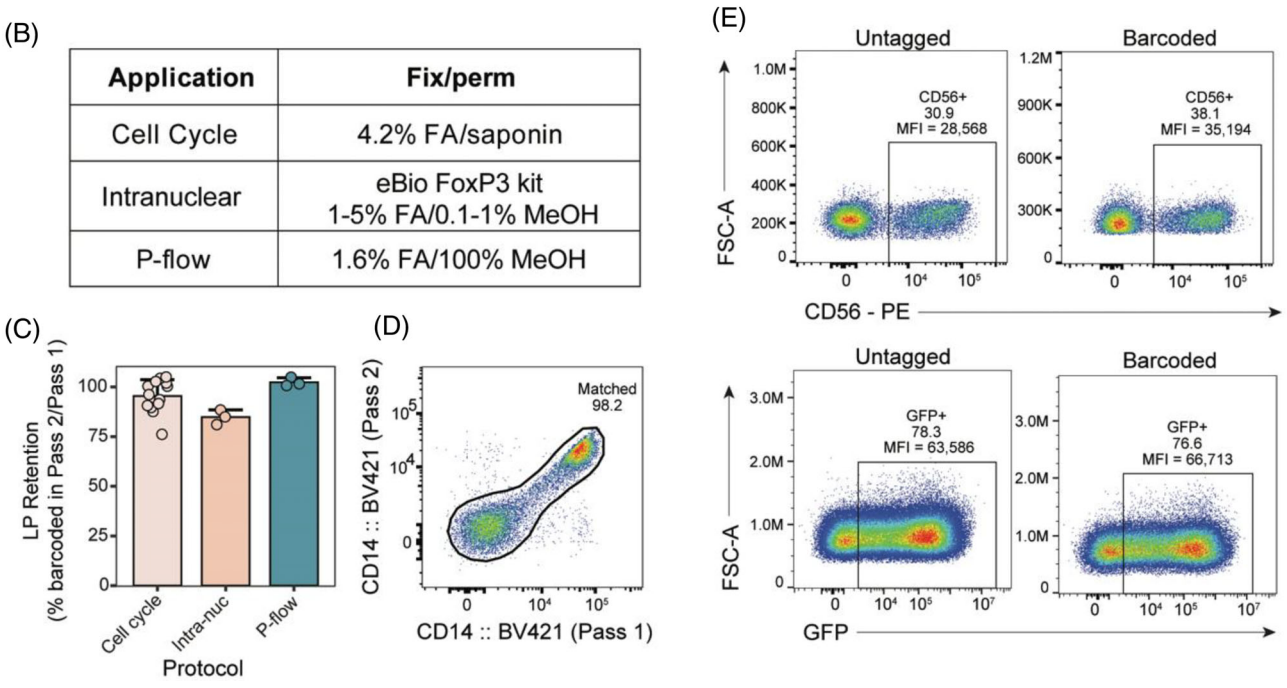

FIGURE 1 Robustness of laser particle (LP) cell barcoding across fix/perm protocols. (A) General schematic of the multi-pass workflow. Cells are typically stained for surface markers, barcoded with LPs, acquired through a LASE multi-pass flow cytometer, captured, fix/perm treated, and re-analyzed. (B) Table showing three applications used for testing barcode stability and their respective fix/perm reagents. (C) Barcode retention in human PBMCs between passes in each application. Retention is calculated as percentage of cells barcoded in Pass 2 relative to the percentage of cells barcoded in Pass 1. (D) CD14 BV421 signals from LP-barcoded human PBMCs before (Pass 1) and after (Pass 2) the application of the phospho-flow (P-flow) protocol. Accurately matched cells with similar signal magnitudes fall along a diagonal axis. (E) Comparison of the fluorescent signals of a surface marker (CD56) and fluorescent protein (GFP) between untagged and barcoded cells from human PBMCs and MCF7 GFP+ cells, respectively. Barcoded cells refers to cells that have been processed through the entire multi-pass workflow shown in (A). FA, formaldehyde; MFI, median fluorescent intensity. [Color figure can be viewed at wileyonlinelibrary.com]

(1) stained with a panel of antibodies targeting surface markers or left untouched to detect FPs, (2) barcoded with LPs, and (3) acquired through a LASE multi-pass flow cytometer equipped with an LP barcode reader and a cell collector [28]. After the cells are captured, (4) they are fixed, permeabilized, and re-stained with intracellular markers, and (5) acquired in a second pass. Multi-pass data from LP-barcoded cells are matched, exported as an FCS file, and processed using conventional flow cytometry software.

We first examined the compatibility of LP barcoding across three commonly used chemically harsh intracellular staining protocols on human PBMCs (Figure 1B). The retention ratios of LP barcodes after various fixation and permeabilization (fix/perm) protocols were measured to be 95.4 ± 8.3% for the cell cycle workflow (4.2% formaldehyde (w/w)), 84.8 ± 3.7% for the intranuclear staining workflow (1–5% formaldehyde (w/w), 0.1–1% methanol (w/w)), and 102.4 ± 2.2% for the phospho-flow workflow (~1.6% formaldehyde (w/w), 90% methanol (w/w)) (Figure 1C). The barcode loss in the intranuclear staining workflow, which utilizes methanol as a strong permeabilizing agent instead of a saponin, a gentler permeabilizer used in standard fix/perm [34, 35], is likely attributed to partial detachment of LPs from

the cell membrane. The accuracy of barcode matching was assessed by comparing the fluorescence intensities from anti-CD14 BV421 (Brilliant Violet 421™) methanol-resistant antibodies stained on a human PBMC sample between the first and second measurements, that is, before and after the fix/perm phospho-flow protocol. A matching accuracy of over 98% was observed (Figure 1D). Finally, the influence of LP-barcoding on surface marker and FP expression was examined. The frequency and median fluorescent intensity (MFI) of surface marker and GFP+ events were within the typical coefficients of variation (CVs <25%) of the assay and cytometry for both LP-barcoded and untagged cells (Figure 1E).

3.2 | Measurement of protein fluorophores before methanol treatment

We developed a two-pass phospho-flow protocol that circumvents the harsh effects of methanol on protein-based fluorophores (Figure 2A) and tested its effectiveness for analyzing PMA/ionomycin-stimulated phosphorylation of ERK1/2 as a model system. Cryopreserved human PBMCs were (1) thawed and stained with viability dye, followed by (2) stimulation with PMA/Ionomycin for 15 min and (3) immediate fixation to preserve the integrity of the phosphorylated protein states. PBMCs were then (4) barcoded with LPs and (5) stained with antibodies conjugated to protein-based fluorophores targeting broad immune cell populations (CD3 PE-Cy5, CD20 APC-Cy7, CD14 BV421, CD56 PE, and HLA-DR PE-Dazzle594). Cells were then (6) acquired through a flow cytometer, captured, (7) permeabilized with 90% ice-cold methanol (v/v), (8) stained intracellularly for p-ERK1/2, and (9) re-acquired in a second pass.

We found that fluorescence from PE- and APC-based fluorophores were significantly reduced or destroyed after methanol permeabilization, consistent with literature reports [26, 36]. This loss of sensitivity resulted in partial (CD20 APC-Cy7) or complete (CD56 PE and CD3 PE-Cy5) inability to identify major cell populations (Figure 2B). In contrast, measuring these markers in the first pass before methanol permeabilization allowed us to identify these markers without the detrimental effects of methanol. In the second pass, the intracellular p-ERK1/2 marker was measured and analyzed with respect to different cell populations identified by the data measured in the first pass prior to methanol permeabilization (Figure 2C). The population percentages and MFI of all fluorophores between barcoded and untagged data were within typical CVs of the assay and cytometer (Figure 2B,C).

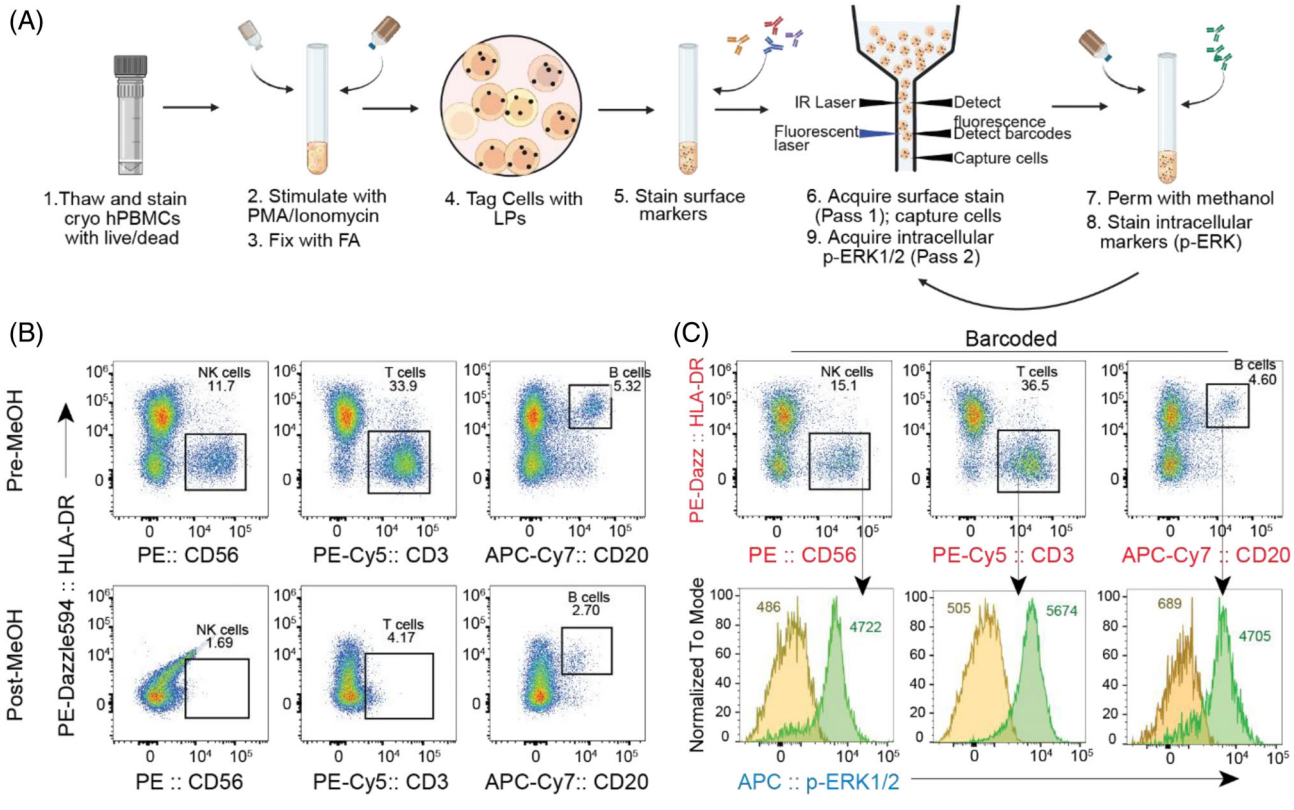

FIGURE 2 Full expression of fluorescence signal measured prior to methanol permeabilization. (A) Schematic of the multi-pass phospho-flow protocol for human PBMCs stimulated with PMA/Ionomycin. (B) Direct comparison of fluorescence from unmatched, barcoded cells before (top) and after (bottom) methanol permeabilization, showing degradation of protein-based fluorophore signals by the MeOH (methanol) treatment. (C) (top) Intact surface marker data acquired in the first-pass (red text) flow cytometry and gating of major cell populations; (bottom) Downstream p-ERK1/2 analysis from intracellular data collected during the second pass (blue text) post fix/perm, gated off barcode-matched, pre fix/perm surface markers. MFI of pERK1/2 signals are shown for non-stimulated (yellow) and stimulated (green). [Color figure can be viewed at wileyonlinelibrary.com]

3.3 | Measurement of sensitive epitopes before methanol permeabilization

Traditionally, phospho-flow studies have been restricted to using small-molecule fluorophores that are resistant to methanol. However, significant issues arise when measuring surface markers that are sensitive to methanol treatment [26, 37–42]. For example, the crucial antigen CD19 is highly susceptible to methanol denaturation. Two common protocols have been developed to partially mitigate this issue: CD19 is stained prior to methanol permeabilization with a methanol-resistant fluorophore (SOP1) [24] or CD19 is stained after methanol permeabilization (SOP2) [43], as illustrated in Figure 3A. We tested four commonly used CD19 antibody clones conjugated to FITC because this fluorochrome is methanol-resistant [39, 41] and commercially available for all clones. However, both approaches are suboptimal and significantly compromise signal quality [43]. Our experiments revealed a large (>75%) failure in detecting CD19+ cells (Figure 3B) due to the denaturation of the CD19 antigen in these protocols.

To solve this problem, we developed a two-pass protocol, which measures CD19 in the first flow pass prior to methanol permeabilization and then intracellular signals in the second pass. The combined data provide the p-ERK1/2 expression levels of all CD19+ cells (Figure 3C). We found no difference in p-ERK1/2 expression between LP-tagged and untagged CD14+ monocytes (Figure 3D).

3.4 | Measurement of fluorescent proteins before fix/perm

Genetically encoded FPs are commonly used to analyze gene insertion and expression, but their stability is vulnerable to fix/perm methods. This poses challenges in accurately quantifying FP expression alongside intracellular marker signals. We used multi-pass flow cytometry to capture complete FP signals before fix/perm and intracellular marker signals after fix/perm, utilizing GFP-expressing MCF7 breast cancer cell lines and GFP/mRFP1 co-expressing murine hematopoietic stem and progenitor cells (HSPCs). Cells were stained with viability dye and/or surface antibody-fluorophores followed by barcoding with LPs (Figure 4A). After the first pass, the collected cells underwent fix/perm using various reagents and protocols, followed by staining with an intracellular cell cycle dye and the second pass.

For MCF7 GFP+ cells, we observed a 50% loss of GFP+ events after employing the intranuclear and phospho-flow protocols. Additionally, more than 10% of GFP+ events were lost during cell cycle

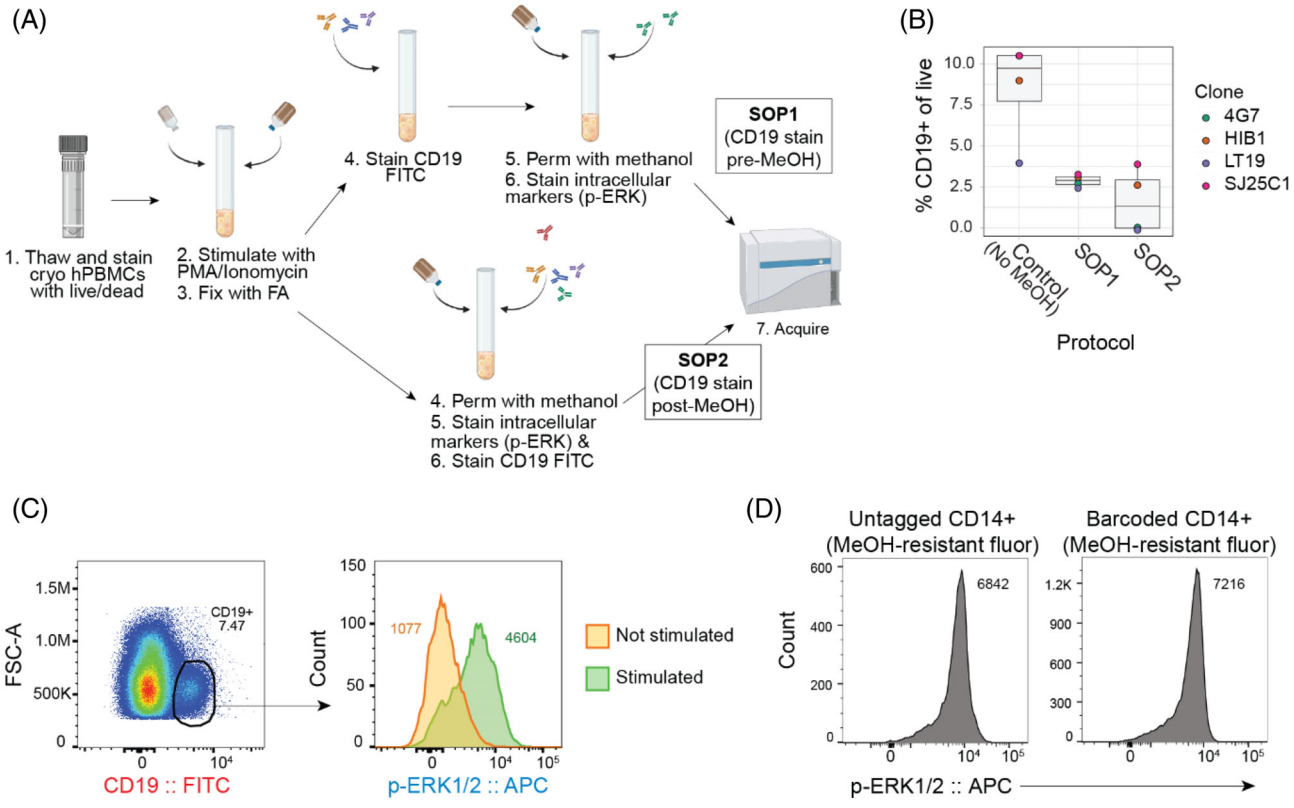

FIGURE 3 Acquisition of CD19 antigen data prior to its destruction by methanol permeabilization. (A) Schematic of two conventional protocols (SOP1 and SOP2) used to detect CD19 expression after fixation and methanol permeabilization. (B) The percentage of CD19+ cells out of total live cells using the conventional methods. (C) (Left) CD19 data acquired in the first pass (red text); (Right) p-ERK1/2 expression acquired during the second pass (blue text) for CD19+ cells identified by the intact CD19 data in the first pass. MFI of the pERK1/2 signals are shown for non-stimulated (yellow) and stimulated populations (green). (D) Comparison of intracellular p-ERK1/2 expression on CD14+ cells stained with methanol-resistant BV421 between untagged and barcoded samples. MFIs of the pERK1/2 signals are listed. [Color figure can be viewed at wileyonlinelibrary.com]

processing (Figure 4B). These protocols also similarly decreased MFIs. One method of retaining GFP expression is through an anti-GFP antibody; however, this approach only partially restored the frequencies to 60–72% of the originals and GFP MFI was significantly reduced (Figure 4B).

Similarly, when applying the cell cycle fix/perm protocol to bone marrow stained to demark immunophenotypic HSPCs, both GFP and mRFP1 signals experienced a significant decrease post fix/perm. Specifically, the MFI of GFP and mRFP1 after fix/perm dropped to 27% and 9% of their original levels, respectively, and differential signal loss between the two FPs was observed. In contrast, measuring FPs prior to fix/perm treatments in our multi-pass workflow fully restored the FP signals (Figure 4C). Therefore, our method allows quantitation of multiple FP expression in combination with intra- and extracellular stains that require fixation/permeabilization.

3.5 | Multi-pass analysis reveals differential fluorescent protein signal loss

Using our model system, we investigated the loss of FP signal due to fix/perm treatments. First, we verified that LP tagging does not alter the expression of intracellular cell cycle signals in MCF7 cells (Figure 5A). Next, using our single-cell barcoding workflow we compared GFP expression in MCF7 cells before and after fix/perm. This comparison confirmed the previously noted losses and identified specific cells that exhibited undetectable levels of GFP in the second pass (Figure 5B, Figure S1). We found that most cells retained less than 50% of the initial GFP signal post-fixation (Figure 5C–E).

Noting the differential loss in GFP and mRFP1 expression in murine HSPCs, we investigated whether FP loss was dependent on cell type. Significant reduction in GFP and mRFP1 intensities were

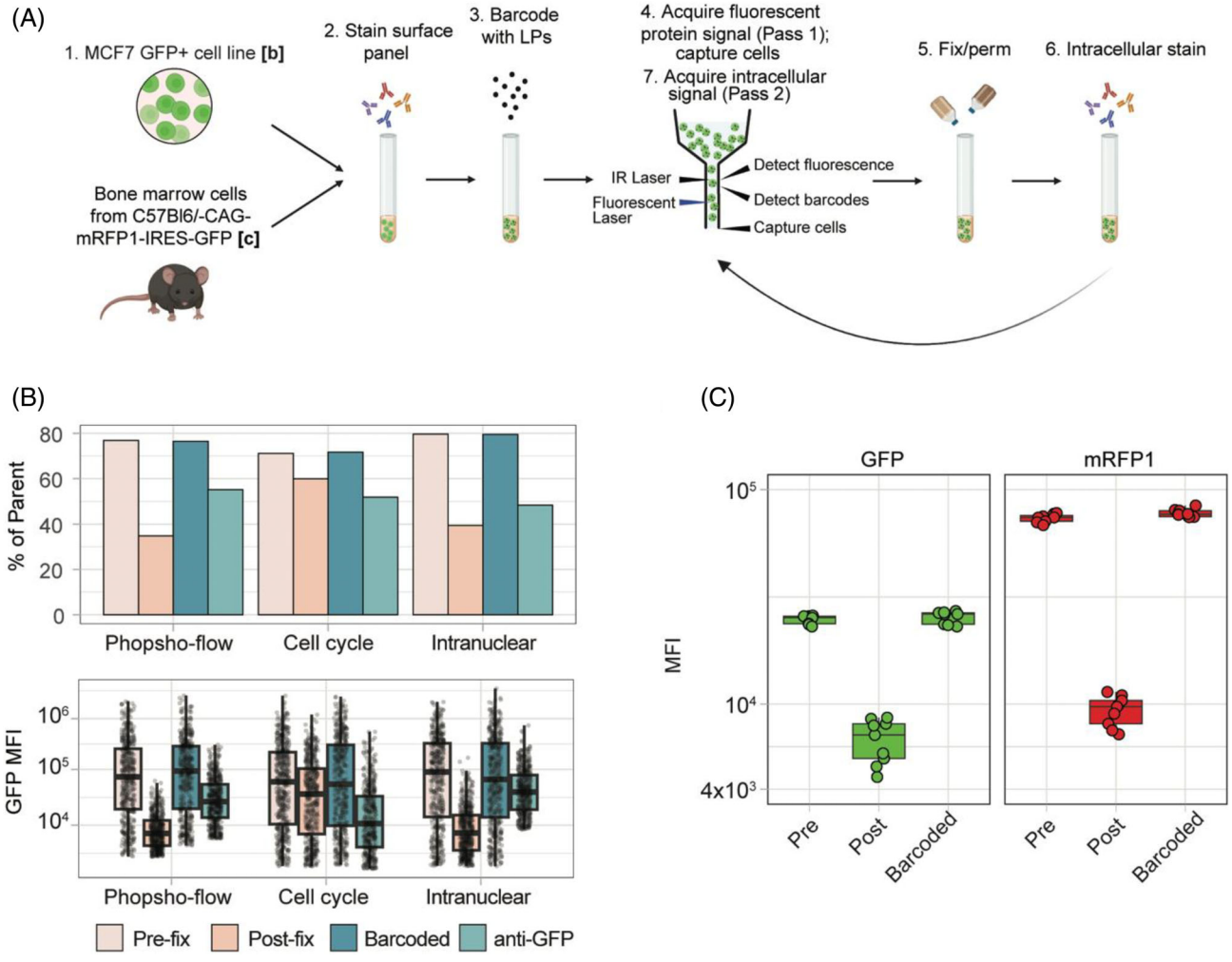

FIGURE 4 Measurement of intact fluorescent protein expression using multi-pass flow cytometry. (A) Schematic of the multi-pass workflow for acquisition of fluorescent protein expression on live cells prior to fix/perm and intracellular stain. (B) Percentage and MFI of GFP from MCF7 GFP+ cells detected pre-fix/perm, post-fix/perm, using two-pass analysis protocol, and using anti-GFP APC following three different fix/perm protocols. Bottom plot shows a box plot of the single cell data with the horizontal line representing median, the box spanning 25th-75th percentile and vertical line spanning minimum to maximum. (C) MFI of GFP/mRFP1 co-expressing bone marrow cells measured before cell cycle fix/perm without barcoding, after fix/perm without barcoding, and with the two-pass protocol with barcoding. Data were collected in triplicate from three mouse donors, with each point representing one replicate. [Color figure can be viewed at wileyonlinelibrary.com]

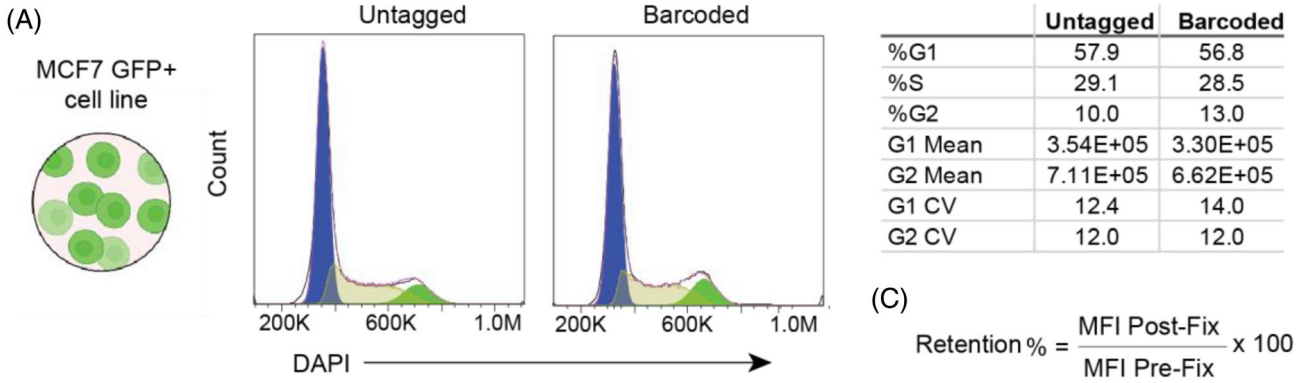

	Untagged	Barcoded
%G1	57.9	56.8
%S	29.1	28.5
%G2	10.0	13.0
G1 Mean	3.54E+05	3.30E+05
G2 Mean	7.11E+05	6.62E+05
G1 CV	12.4	14.0
G2 CV	12.0	12.0

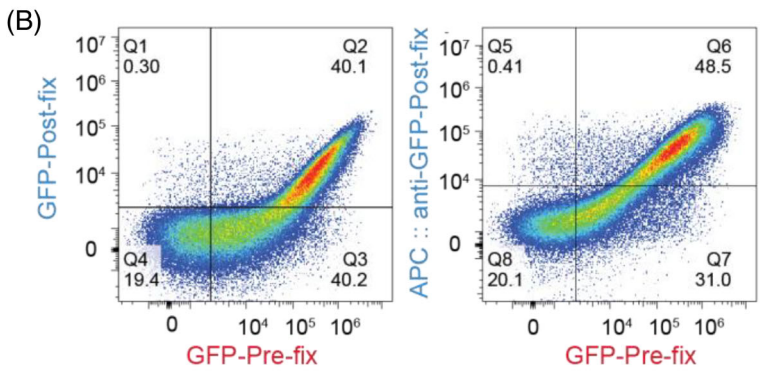

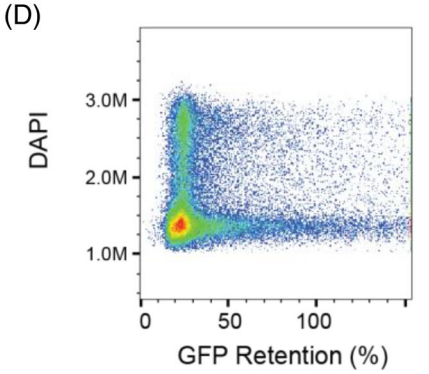

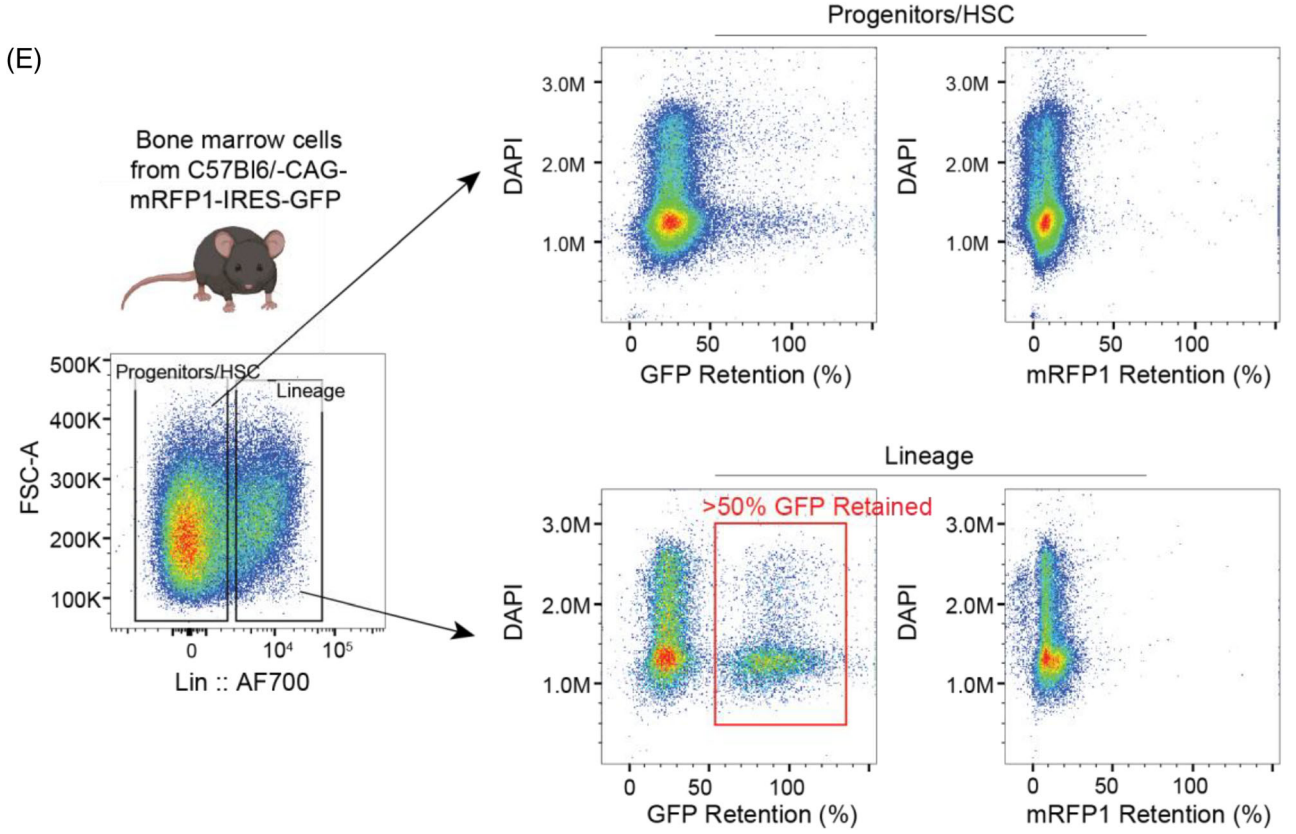

FIGURE 5 Legend on next page.

observed among both HSPCs (Figure 5E, Figure S1). However, we observed a distinct cell population among lineage-positive cells that maintained a similar amount of GFP expression across passes, which was not observed with mRFP1. These results highlight a potential source of bias if FP signals are only quantified post fix/perm.

4 | DISCUSSION

In flow cytometry, detecting each marker type often requires specific sample processing methods that may interfere with the detection of other markers. This issue frequently arises in immune-oncology and stem cell biology research. For example, detecting phosphorylated signaling proteins and fragile surface markers on the same cells is essential for studying cell division and survival in cancer, but methanol permeabilization required for phospho-flow can degrade surface markers needed for phenotyping [3]. To address this problem, researchers often optimize fixative concentrations and incubation times to enable simultaneous detection of both types of markers. However, this approach inevitably compromises signal quality for each marker type, ultimately reducing assay sensitivity [21, 24, 25]. Another strategy involves designing panels using only methanol-resistant fluorochromes (such as BV fluorochromes) and epitopes, but this complicates and limits panel design by restricting reagent options and may necessitate the exclusion of important markers [27]. Alternatively, pre-sorting cells based on surface marker expression, followed by intracellular staining and re-acquisition is sometimes used. However, this method is time-intensive and costly, and impractical for sorting many cell types at once, leading to the loss of single-cell data collected during sorting.

We have presented a novel multi-pass approach that resolves this previous dilemma by enabling separate flow measurements of different markers. Optical barcoding using stable LPs allows repeated measurements of the same cells. Instead of measuring every marker of interest simultaneously, cells can be acquired before and after each cell processing step, with the resulting data from each pass integrated for each cell via barcoding. This allows workflows optimized for the detection of each marker type to be used without compromise. Our approach is similar in principle to fluorescence imaging methods that rely on iterative imaging cycles to capture additional parameters with each cycle. This strategy previously was not applicable to flow cytometry since unlike imaging, cell identity is usually lost with each cycle of flow acquisition. To our knowledge, LP barcoding is the only method that enables non-invasive tracking of millions of cells over multiple measurements [44, 45].

We demonstrated several applications of our approach. First, we showed surface phenotyping of stimulated human PBMCs combined with the detection of phosphorylated protein p-ERK1/2 by acquiring cells before and after methanol permeabilization. Second, we showed detection of FP expression from MCF7 and mouse bone marrow cells combined with intracellular cell cycle staining by acquiring cells before and after fixation and permeabilization. In both cases, samples processed through the multi-pass workflow produced a single FCS file that integrated single-cell data from fix/perm-incompatible signals obtained during the first pass (FPs, sensitive fluorochromes, and fragile epitopes) with cell cycle or phosphorylation data acquired in the second pass. For all workflows, we established the stability of barcoding and confirmed that LP tagging did not influence the detection or quality of FP or intracellular data. The loss of GFP and mRFP1 with fix/perm appears to be dependent on FP type, cell type, and cell cycle stage.

Detailed validation of the multi-pass flow cytometry method will be needed once the LP-reading cytometer is fully available commercially. This includes assessment of assay precision to ensure repeatability across aliquots and operators, assay specificity to identify acceptable criteria for background noise, and assay sensitivity to identify the lowest frequency of cells that can be distinguished. These metrics generally apply to any novel flow cytometry-based assay, but unique in this case will be repeatability, yield, and stability of LP barcoding. As we have shown in this manuscript, it will also be important to compare multi-pass data with data acquired in separate passes to ensure no significant changes in marker signal due to LP barcoding.

Our multi-pass flow cytometry approach allows for flexible and simplified panel design through unencumbered fluorochrome and epitope choice, and significant savings on resources spent optimizing assay-specific parameters, including antibody clones, fluorochromes, buffers, reagent concentrations, and workflows. We anticipate this method will facilitate unprecedented cellular analysis from phenotype to state to function through optimized detection of different marker types on the same cells.

AUTHOR CONTRIBUTIONS

Marissa D. Fahlberg: Conceptualization; methodology; data curation; supervision; formal analysis; writing – original draft; writing – review and editing; visualization; validation. **Sarah Forward:** Investigation; writing – review and editing; methodology; data curation; project administration; validation. **Emane Rose Assita:** Investigation; methodology; writing – review and editing; validation. **Michael Mazzola:** Conceptualization; writing – review and editing; methodology; investigation; resources; validation. **Anna Kiem:** Investigation; resources. **Maris Handley:** Conceptualization; writing – review and

FIGURE 5 Fluorescent protein signal loss differs by cell type and cell cycle stage. (A) Representative histograms comparing DAPI staining on untagged and LP-tagged MCF7 GFP+ cells. (B) Direct comparison of GFP expression from MCF7 cells before and after fix/perm (intranuclear protocol) and relative to the anti-GFP antibody stained after fix/perm. Red text highlights data collected in the first pass, and blue text represents data collected in the second pass. (C) Calculation of Retention %, a metric quantifying fluorescent protein loss post-fixation relative to pre-fixation. (D) Representative dot plot showing the GFP signal change between the first and second passes. Most cells significantly lost GFP signals in the second pass after fix/perm. (E) (Left) marker gating data and the loss of GFP and mRFP1 across (top) hematopoietic progenitors and stem cells (HSC) and (bottom) lineage+ populations before and after fix/perm. [Color figure can be viewed at wileyonlinelibrary.com]

editing; methodology; resources. **Seok-Hyun Yun:** Writing – review and editing. **Sheldon J. J. Kwok:** Conceptualization; funding acquisition; writing – original draft; writing – review and editing; methodology; formal analysis; project administration; supervision; data curation; visualization; resources.

ACKNOWLEDGMENTS

M. F., S .F., E. A., S. H. Y., and S. J. J. K. have financial interests in LASE Innovation Inc., a company focused on commercializing technologies based on optical barcodes. The financial interests of S. H. Y. were reviewed and are managed by Massachusetts General Brigham in accordance with their conflict-of-interest policies.

FUNDING INFORMATION

This work was supported in part by grants from the National Institutes of Health (R44-GM139504, R43-GM140527, and R01-EB033155). M. M. was funded by National Institutes of Health (F31HL158020-03, T32GM132089-01, and 5T32GM007226-43).

ORCID

Sheldon J. J. Kwok https://orcid.org/0000-0001-7880-0401

REFERENCES

1. Uno N, Kaku N, Morinaga Y, Hasegawa H, Yanagihara K. Flow cytometry assay for the detection of single-copy DNA in human lymphocytes. Nucleic Acids Res. 2020;48:e86.
2. Kim KH, Sederstrom JM. Assaying cell cycle status using flow cytometry. Curr Protoc Mol Biol. 2015;111:28.6.1–28.6.11.
3. Schulz KR, Danna EA, Krutzik PO, Nolan GP. Single-cell phospho-protein analysis by flow cytometry. Curr Protoc Immunol. 2012;8:8.17.1–8.17.20.
4. Krutzik PO, Nolan GP. Intracellular phospho-protein staining techniques for flow cytometry: monitoring single cell signaling events. Cytometry A. 2003;55:61–70.
5. Yin Y, Mitson-Salazar A, Prussin C. Detection of intracellular cytokines by flow cytometry. Curr Protoc Immunol. 2015;110:6.24.1–6.24.18.
6. Vora AA, Mondala PK, Costello C, MacLeod AR, Crews LA. Sensitive intranuclear flow cytometric quantification of IRF4 protein in multiple myeloma and normal human hematopoietic cells. STAR Protoc. 2021;2:100565.
7. Rothaeusler K, Baumgarth N. Evaluation of intranuclear BrdU detection procedures for use in multicolor flow cytometry. Cytometry A. 2006;69:249–59.
8. Arrigucci R, Bushkin Y, Radford F, Lakehal K, Vir P, Pine R, et al. FISH-flow, a protocol for the concurrent detection of mRNA and protein in single cells using fluorescence in situ hybridization and flow cytometry. Nat Protoc. 2017;12:1245–60.
9. Hawley TS, Hawley RG, Telford WG. Fluorescent proteins for flow cytometry. Curr Protoc Cytom. 2017;80:9.12.1–9.12.20.
10. Galbraith DW, Anderson MT, Herzenberg LA. Flow cytometric analysis and FACS sorting of cells based on GFP accumulation. Methods Cell Biol. 1999;58:315–41.
11. Yin T, Wang G, Wang L, Mudgal P, Wang E, Pan CC, et al. Breaking NGF–TrkA immunosuppression in melanoma sensitizes immunotherapy for durable memory T cell protection. Nat Immunol. 2024;25:268–81.
12. Chen Y, Chen X, Bao W, Liu G, Wei W, Ping Y. An oncolytic virus–T cell chimera for cancer immunotherapy. Nat Biotechnol. 2024;1–12.
13. Davies D, Kamdar S, Woolf R, Zlatareva I, Iannitto ML, Morton C, et al. PD-1 defines a distinct, functional, tissue-adapted state in Vδ1+ T cells with implications for cancer immunotherapy. Nat Cancer. 2024;5:420–32.
14. Chang Y, Bach L, Hasiuk M, Wen L, Elmzzahi T, Tsui C, et al. TGF-β specifies TFH versus TH17 cell fates in murine CD4+ T cells through c-Maf. Sci Immunol. 2024;9:eadd4818.
15. van Gastel N, Stegen S, Eelen G, Schoors S, Carlier A, Daniëls VW, et al. Lipid availability determines fate of skeletal progenitor cells via SOX9. Nature. 2020;579:111–7.
16. Sun J, Hu L, Bok S, Yallowitz AR, Cung M, McCormick J, et al. A vertebral skeletal stem cell lineage driving metastasis. Nature. 2023;621:602–9.
17. Zou D, Yin Z, Yi SG, Wang G, Guo Y, Xiao X, et al. CD4+ T cell immunity is dependent on an intrinsic stem-like program. Nat Immunol. 2024;25:66–76.
18. Rao S, Lungu C, Crespo R, Steijaert TH, Gorska A, Palstra RJ, et al. Selective cell death in HIV-1-infected cells by DDX3 inhibitors leads to depletion of the inducible reservoir. Nat Commun. 2021;12:2475.
19. Djeghloul D, Dimond A, Cheriyamkunnel S, Kramer H, Patel B, Brown K, et al. Loss of H3K9 trimethylation alters chromosome compaction and transcription factor retention during mitosis. Nat Struct Mol Biol. 2023;30:489–501.
20. Cao M, Chen P, Peng B, Cheng Y, Xie J, Hou Z, et al. The transcription factor ELF4 alleviates inflammatory bowel disease by activating IL1RN transcription, suppressing inflammatory TH17 cell activity, and inducing macrophage M2 polarization. Front Immunol. 2023;14:1270411.
21. Heinen AP, Wanke F, Moos S, Attig S, Luche H, Pal PP, et al. Improved method to retain cytosolic reporter protein fluorescence while staining for nuclear proteins. Cytometry A. 2014;85:621–7.
22. Ottens K, Schneider J, Satterthwaite AB. T-bet-expressing B cells contribute to the autoreactive plasma cell pool in Lyn−/− mice. Eur J Immunol. 2023;53:e2250300.
23. Kos K, Salvagno C, Wellenstein MD, Aslam MA, Meijer DA, Hau CS, et al. Tumor-associated macrophages promote intratumoral conversion of conventional CD4+ T cells into regulatory T cells via PD-1 signalling. Onco Targets Ther. 2022;11:2063225.
24. Zwang NA, Ganesh BB, Cardenas KT, Chong AS, Finn PW, Perkins DL. An optimized protocol to quantify signaling in human transitional B cells by phospho flow cytometry. J Immunol Methods. 2018;463:112–21.
25. Rip J, de Bruijn MJW, Kaptein A, Hendriks RW, Corneth OBJ. Phosphoflow protocol for signaling studies in human and murine B cell subpopulations. J Immunol. 2020;204:2852–63.
26. Krollmann C, Cieslak K, Koerber RM, Luksch H, Rösen-Wolff A, Brossart P, et al. Quantification of unperturbed phosphoprotein levels in immune cell subsets with phosphoflow to assess immune signaling in autoimmune disease. STAR Protoc. 2022;3:101309.
27. Marsman C, Jorritsma T, Ten Brinke A, van Ham SM. Flow Cytometric methods for the detection of intracellular signaling proteins and transcription factors reveal heterogeneity in differentiating human B cell subsets. Cells. 2020;9 :2633.
28. Kwok SJJ, Forward S, Fahlberg MD, Assita ER, Cosgriff S, Lee SH, et al. High-dimensional multi-pass flow cytometry via spectrally encoded cellular barcoding. Nat Biomed Eng. 2024;8:310–24.
29. Martino N, Kwok SJJ, Liapis AC, Forward S, Jang H, Kim HM, et al. Wavelength-encoded laser particles for massively multiplexed cell tagging. Nat Photonics. 2019;13:720–7.
30. Mazzola M, Zhao T, Gustafsson K, Kristiansen T, Schiroli G, Milosevic J, et al. Cap-independent protein translation in hematopoiesis. Blood. 2022;140:1983–4.
31. R Core Team. R: a language and environment for statistical computing. Vienna, Austria: R Foundation for Statistical Computing; 2023.

32. Wickham H, Averick M, Bryan J, Chang W, McGowan L, François R, et al. Welcome to the tidyverse. J Open Source Software. 2019;4:1686. https://doi.org/10.21105/joss.01686
33. Van P, Jiang W, Gottardo R, Finak G. Ggcyto: next-generation open-source visualization software for cytometry. Bioinformatics. 2018;34:3951–3. https://doi.org/10.1093/bioinformatics/bty441
34. Zheng X, Gallot G. Dynamics of cell membrane permeabilization by saponins using terahertz attenuated total reflection. Biophys J. 2020;119:749–55.
35. Jamur MC, Oliver C. Permeabilization of cell membranes. Immunocytochemical methods and protocols. Totowa, NJ: Humana Press; 2010.
36. Spurgeon BEJ, Naseem KM. Phosphoflow cytometry and barcoding in blood platelets: technical and analytical considerations. Cytometry B Clin Cytom. 2020;98:123–30.
37. Intracellular flow cytometry protocol using alcohol. Novus Biologicals https://www.novusbio.com/support/support-by-application/general-intracellular-cytoplasmic-target-flow-protocol-using-alcohol (2015).
38. Protocol compatibility for immune signaling and phenotyping by flow cytometry. Cell Signaling Technology. https://www.cellsignal.com/learn-and-support/reference-tables/flow-protocol-compatibility
39. 3 considerations for intracellular flow cytometry (ICFC). Biol Theory. https://www.biolegend.com/nl-nl/blog/3-considerations-for-intracellular-flow-cytometry-icfc
40. Antibody fixation considerations. ThermoFisher. https://www.thermofisher.com/us/en/home/life-science/cell-analysis/cell-analysis-learning-center/cell-analysis-resource-library/ebioscience-resources/antibody-fixation-considerations.html
41. BestProtocols: staining intracellular antigens for flow cytometry. ThermoFisher. https://www.thermofisher.com/us/en/home/references/protocols/cell-and-tissue-analysis/protocols/staining-intracellular-antigens-flow-cytometry.html.
42. Chow S, Hedley D, Grom P, Magari R, Jacobberger JW, Shankey TV. Whole blood fixation and permeabilization protocol with red blood cell lysis for flow cytometry of intracellular phosphorylated epitopes in leukocyte subpopulations. Cytometry A. 2005;67:4–17.
43. Mavropoulos A, Bogdanos DP, Liaskos C, Orfanidou T, Simopoulou T, Zafiriou E, et al. Flow cytometric detection of p38 MAPK phosphorylation and intracellular cytokine expression in peripheral blood subpopulations from patients with autoimmune rheumatic diseases. J Immunol Res. 2014;2014:671431.
44. Alieva M, Wezenaar AKL, Wehrens EJ, Rios AC. Bridging live-cell imaging and next-generation cancer treatment. Nat Rev Cancer. 2023;23:731–45.
45. Kwok SJJ, Martino N, Dannenberg PH, Yun S-H. Multiplexed laser particles for spatially resolved single-cell analysis. Light Sci Appl. 2019;8:74.

SUPPORTING INFORMATION

Additional supporting information can be found online in the Supporting Information section at the end of this article.

How to cite this article: Fahlberg MD, Forward S, Assita ER, Mazzola M, Kiem A, Handley M, et al. Overcoming fixation and permeabilization challenges in flow cytometry by optical barcoding and multi-pass acquisition. Cytometry. 2024. https://doi.org/10.1002/cyto.a.24904